Electrochimica Acta 189 (2016) 184–189

Contents lists available at ScienceDirect

Electrochimica Acta

journal homepage: www.elsevier.com/locate/electacta

Highly stable and flexible ITO-free electrochromic films with bi-functional stacked MoO_3/Ag/MoO_3 structures

Yan Liu[a,b], Ying Lv[a,*], Zhaobing Tang[a,b], Longgui He[c], Xingyuan Liu[a,*]

[a] State Key Laboratory of Luminescence and Applications, Changchun Institute of Optics, Fine Mechanics and Physics, Chinese Academy of Sciences, Changchun 130033, China
[b] University of Chinese Academy of Sciences, Beijing 100049, China
[c] Fujian Jiechuang Electronic Technology Co., Ltd., Fuqing 350301, China

ARTICLE INFO

Article history:
Received 26 August 2015
Received in revised form 2 December 2015
Accepted 16 December 2015
Available online 19 December 2015

Keywords:
Electrochromism
Flexible
Dielectric-metal-dielectric
Durability
MoO_3.

ABSTRACT

Stacked MoO_3/Ag/MoO_3 (MAM) films, which can serve as both transparent electrodes and electrochromic materials, were utilized for constructing high-performance flexible indium tin oxide (ITO)-free electrochromic devices. Compared with the more common modif of MoO_3 on ITO, a faster response time, greater optical contrast, higher coloration efficiency, and better electrochemical and mechanical durability were achieved with the use of MAM films.

1. Introduction

Electrochromism is the phenomenon of controllable and reversible changes in optical properties caused by electrochemically induced redox reactions [1,2]. The advantages of electrochromic devices (ECDs) over more well-established polymer dispersed liquid crystal devices are their low material cost and compatibility with nonplanar and flexible surfaces. Owing to these, ECDs show considerable promise for applications in lightweight goggles, implantable displays, and wearable electronic textiles [3–5]. However, the development of flexible ECDs is still a challenge due to the limited availability of flexible transparent conductive films and electrochromic (EC) materials with the desired photoelectrical properties and durability. Indium tin oxide (ITO) on a polyethylene terephthalate (PET) substrate is the most commonly used flexible electrode material, but its brittleness and high-temperature processing requirements limit its use in flexible devices [6,7]. Recently, graphene and conducting polymer alternatives to ITO (such as PEDOT) has been used for flexible ECD materials [8,9]. However, electrodes fabricated from these materials suffer from low transmittance in the bleached state. Metal grids and Ag nanowires, which display good flexibility and high conductivity, have also been drawn onto flexible ECDs. However, these particular ECDs often exhibit inhomogeneous color change or "blooming" effects, and have only modest durability because of the different resistances of the metal lines and the spaces between them [10,11].

One way to resolve these problems is to use a dielectric-metal-dielectric (DMD) structure to construct a transparent electrode [12], which combines high optical transmittance with a uniform high conductivity. Ag thin films (<20 nm thick) are commonly used as the middle layer in such systems, due to having low resistance and high transmittance in the visible region. Various dielectric materials such as WO_3, ZnS, and TiO_2 have also been evaluated as candidate materials for use in DMD structures [12]. This DMD structure has been widely used in electrodes in organic optoelectronic devices, such as light emitting diodes [13] and organic solar cells [14,15]. Unfortunately, there are few reports on the utilization of DMD layered structures as conductive electrodes in ECDs [16]. High optical transmittance and high conductivity can be easily realized in DMDs on flexible substrates that utilize more abundant indium-free materials as the dielectric, making a DMD a low-cost and more practical flexible transparent electrode. Moreover, by employing high performance EC materials as the outer dielectric layer (such as WO_3 or TiO_2), one can integrate the electrode and EC bi-functionality into one DMD structured device, simplifying ECD construction and reducing fabrication costs by using an EC dielectric layer with a thickness on the order of 10^1 nm. Recently,

* Corresponding authors.
E-mail addresses: lvying@ciomp.ac.cn (Y. Lv), liuxy@ciomp.ac.cn (X. Liu).

http://dx.doi.org/10.1016/j.electacta.2015.12.115
0013-4686/

we have realized a high performance rigid ECD utilizing a WO_3/Ag/WO_3 (WAW) film as both a transparent conductor and an EC material [16]. However, the obtained flexible WAW film exhibited defective EC performance at long response times, as well as low optical contrast and inferior durability, which could be attributed to the substantially rough surface morphology of the flexible WAW film and its relatively large sheet resistance.

In this study, we demonstrate the use of MoO_3, one of the most well-studied EC materials, as a dielectric material in the construction of a flexible dual-functional (transparent electrode and EC functions) MoO_3/Ag/MoO_3 (MAM) film on PET for high performance ITO-free, flexible ECDs. MoO_3 was chosen because of its unique combination of favorable chemical and environment stability and outstanding optical modulation properties [17,18]. Moreover, compared with WO_3 films, the EC response of MoO_3 shows a stronger and more uniform absorption of light in its colored state, as well as a better open-circuit memory effect [19–21]. By adjusting the thickness of each layer, the optimized MAM films exhibit excellent electrical, optical, and mechanical properties, together with a fast optical response time and high coloration efficiency. Most importantly, a dramatic enhancement in the cycling stability of the MoO_3 films is achieved with this stacked MAM structure. This indicates that the transparent conductor and EC bi-functional MAM film is a prominent candidate for use in high-performance flexible ECDs.

2. Experimental

2.1. Fabrication of MAM films

The MAM films were deposited at room temperature onto the cleaned glass and PET substrates by electron-beam evaporation. The inner MoO_3 layer (closest to the substrate) was deposited by ion-beam-assisted electron-beam evaporation in order to enhance the adhesive quality of the MoO_3 layer to the substrate and to obtain a smooth and compact MoO_3 thin layer. It has been demonstrated that the use of ion-beam-assisted deposition can improve film morphology, reduce optical scatting, and ameliorate the optical properties of many materials [22,23]. The obtained smooth inner MoO_3 layer was also beneficial for improving the surface features of the subsequent Ag and outer MoO_3 layers, and highly uniform and smooth MAM films were achieved after deposition of these layers. Prior to deposition, the glass and PET substrates were ultrasonically cleaned with acetone, ethanol, and deionized water for 10 min successively, and finally dried in an oven. The evaporation rates of MoO_3 and Ag were 0.1–0.2 and 0.7–1.0 nm s^{-1}, respectively, at pressures $<3 \times 10^{-3}$ Pa. During the deposition of the inner MoO_3 layer, the chamber was flushed with Ar gas to maintain a working pressure of 3.0×10^{-2} Pa. An end-Hall ion beam operating at an anode voltage of 80 V was used to assist deposition. Monolayer MoO_3 was also prepared on a PET/ITO substrate for comparison.

2.2. Characterization

The film thicknesses were calibrated with an Ambios XP-1 surface profiler. The optical constants of MoO_3 and Ag films used in the simulations were acquired using a from an HORIBA Jobin Yvon ellipsometer. The transmittance spectra of the films were evaluated using a Shimadzu UV-3101PC spectrophotometer. The crystal structures of the MAM films were determined by X-ray diffraction (XRD, D8 Focus, Bruker, Germany) analysis. The surface resistances of the films were measured using a four-point probe instrument. The bending properties of the flexible MAM films were investigated using a home-made cyclic bending test system at a bending radius of 11 mm. Atomic force microscopy (AFM) measurements were performed on a Shimadzu SPM-7900 (tapping mode) instrument, and optical microscopy images were recorded using an Olympus BX51TRF microscope.

2.3. EC measurements

All of the electrochemical measurements were obtained using a CHI 920 electrochemical workstation (Shanghai Chenhua Instruments Inc., China) equipped with a Maya 2000 spectrometer with a scan range of 380–820 nm. The EC properties of the films were measured using a standard three-electrode system, with MAM or PET/ITO/MoO_3 (ITOM) as the working electrode (18 mm × 18 mm), a titanium plate as the counter electrode (5 mm × 20 mm), and Ag/AgCl (3.5 M KCl) as the reference electrode. A 1 M $LiClO_4$ solution in propylene carbonate (PC) was used as the electrolyte, which was degassed with nitrogen for 30 min prior to each test; analytical grade $LiClO_4$ and PC were both purchased from Sigma-Aldrich. All measurements were performed in air at room temperature.

3. Results and discussion

3.1. Thickness optimization

The optical and electrical properties of the DMD structures depend on the thickness of each layer [15,24–26]. The threshold thickness value of the metal layer is normally around 10 nm, above which a DMD structure typically changes from an insulating state to a highly conductive state. This change is attributed to the percolation of conducting metal paths [15,26,27]. Therefore, an

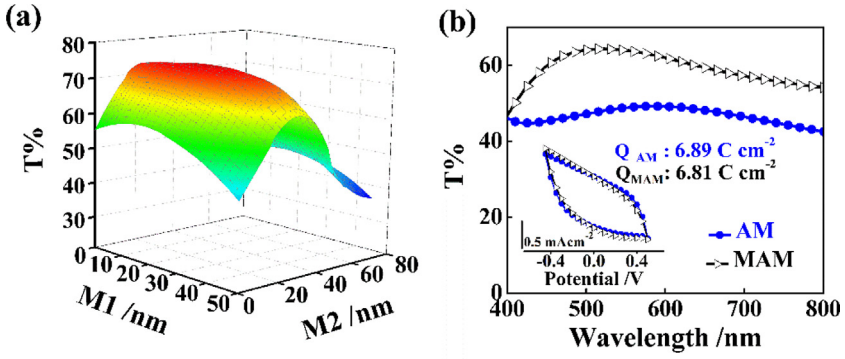

Fig. 1. (a) Calculated average transmittance (400–800 nm) of glass/MAM structures as functions of thickness of two MoO_3 layers, Ag thickness is fixed at 11 nm; (b) Measured transmittance of as-prepared MAM (30/11/50 nm) and Ag/MoO_3 (AM, 11/50 nm) films on glass. The inset image shows the cyclic voltammetry curves of the MAM and AM films with a scan rate of 0.1 V s^{-1} and scan range of –0.45–0.5 V (vs. Ag/AgCl).

11–nm–thick Ag layer was introduced to ensure a low sheet resistance, while the thicknesses of the two MoO_3 layers were varied in order to optimize the optical transmittance of the MAM films on glass. Hereafter, the inner and the outer MoO_3 layers in our MAM structures are referred to as M1 and M2, respectively. Fig. 1a shows the simulated average transmittance (400–800 nm) of MAM films with various M1 and M2 thicknesses, collected using an optical transfer matrix method (calculation details can be found in the Supporting Information in Table S1). It can be observed that the transmittances of the MAM films can be precisely modulated by simply changing the thickness of the two MoO_3 layers. Increasing the MoO_3 thicknesses increases the average transmittance of the MAM films, which then decreases after reaching a maximum value of 74.5% for the 30/11/30–nm–thick MAM film. The measured transmittance spectra of MAM films with different MoO_3 thicknesses are in good agreement with these calculated results (Fig. S1). The best MAM (30/11/30) film performance presented a maximum transmittance of 83.9% at 512 nm and an average transmittance of 78.0% over the wavelength range of 400–800 nm.

It should be noted that without the M1 layer, the mean transmittance of Ag/MoO_3 (here after referred as AM, 11/50 nm) in the visible region (400–800 nm) was only 47%, which was significantly enhanced by 30% (reaching a value of 60%) over the same range after inserting the 30 nm M1 layer (Fig. 1b). The high transmittance for the MAM film was favorable for some special applications such as in displays and smart windows. The charge insertion/extraction behavior of MAM and AM films were studied using electrochemical cyclic voltammetry (CV) methods. It was found that the CV curves and the injected charge densities of the MAM and AM films under the same conditions were nearly identical (6.81 vs. 6.89 C cm^{-2},Fig. 1b inset), suggesting that the presence of the inner MoO_3 has almost no effect on the electrochemical redox, but instead is critical for achieving high transmittance in the electrode and EC bilayer. In other words, the EC properties appear to mainly depend on the outer MoO_3 dielectric layer.

In order to evaluate the effect of M2 thickness on the EC performance of MAM films, potential step chronoamperometric experiments were performed while simultaneously recording the changes of the transmittance at 528 nm at each step. The optical contrast (ΔT) and response time (τ) of the MAM films were systematically evaluated (Fig. 2 and Table S2). The vertical error bar in Fig. 2 indicates the standard error of four independent experiments. When the potential was switched from –0.45 V to 0.5 V (vs. Ag/AgCl), all MAM films exhibit EC behavior with a reversible color change from dark blue to light blue, which can be correlated with the intercalation and de-intercalation of electrons from the electrode and Li^+ ions from the electrolyte, respectively. Nevertheless, significant differences were observed in the optical properties of these MAM films. As the M2 thickness is increased from 30 to 70 nm, the transmittance at 528 nm in the bleached state gradually decreases from 73% to 57%. However, the optical contrast ($\Delta T = T_b - T_c$, where T_b represents the transmittance in the bleached state and T_c represents the transmittance in the colored state) of the MAM films at the same wavelength increases and then slightly decreases after reaching a maximum value of 28.6 ± 1.7% for 50–nm –thick M2 layer (Fig. 2a). As shown in Fig. 2b, there is no clear trend in response time as a function of outer MoO_3 layer thickness. For the (30/11/50 nm) MAM structure, the derived coloration and bleaching response time for a 90% transmittance change were found to be 7.0 ± 0.9 s (τ_c, coloration time) and 9.5 ± 1.7 s (τ_b, bleaching time). By further increasing the thickness of M2 to 70 nm, the maximum optical contrast of the MAM film reached 26.8 ± 2.3%. However, this film exhibited a longer response time (τ_c = 9.9 ± 0.7 s, τ_b = 18.8 ± 1.8 s). Therefore, the MAM with a 50 nm outer MoO_3 layer was chosen for further study. The difference in response time of these MAM films with various thicknesses may be related to the solid state diffusion of Li^+ in the oxide particles as well as the interfacial processes [28,29].

3.2. EC performance of flexible MAM films

Based on the results of the above analysis, we further studied the EC properties of flexible MAM (30/11/50 nm) films on PET substrates, with ITOM films (11/50 nm and 11/100 nm) also prepared for comparison. The optical contrast of the flexible MAM film could be controlled by adjusting the applied potential. As the potential ranged from ±0.15 to ±0.6 V, the optical contrast of MAM at 528 nm was significantly enhanced from < 5% to more than 20% (Fig. S2 in the Supporting Information). Moreover, the open-circuit memory effect for the MAM is favorable, and these optical properties are maintained for more than 24 h. From Fig. 3, we see that the flexible MAM film demonstrates faster response times (τ_c = 6.2 s, τ_b = 10.9 s) and a significantly stronger optical modulation of 27.7% at 528 nm in comparison to that of the ITOM film (11/50 nm, τ_c = 10.4 s, τ_b = 17.7 s, ΔT = 9.3%). Even in the wavelength range of 500–800 nm, the average optical contrast for the MAM films can reach 26.2% (Fig. S3a). More importantly, the optical contrast of the MAM film with the 50 nm outer MoO_3 layer is even greater than that of the 100–nm–thick MoO_3 layer on the ITO electrode (21.3%, Fig. S3b). In addition, the EC performance of the flexible MAM films was comparable to that of a more rigid MAM film, demonstrating a distinct advantage over previously reported flexible WAW films [16].

The microstructure, surface morphology and the homogeneity of the MAMs were measured using XRD and AFM. XRD analysis

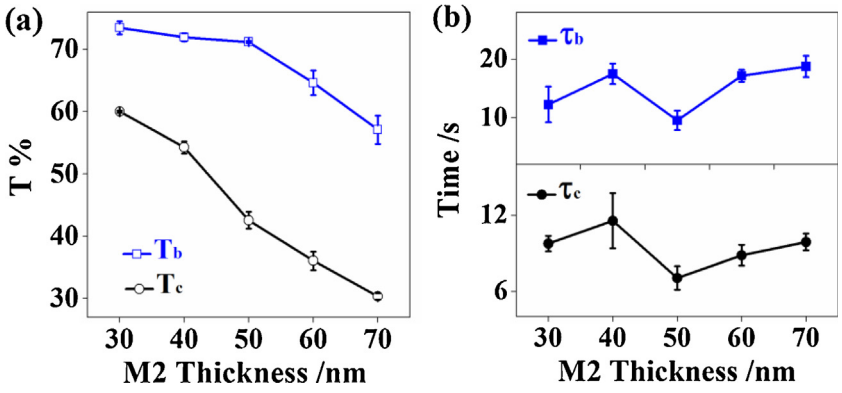

Fig. 2. (a) Optical contrast at 528 nm and (b) response time of glass/MAM (30/11/x nm) films in bleached and colored states as a function of x, at potential steps from 0.5 V (40 s) to –0.45 V (50 s, vs. Ag/AgCl).

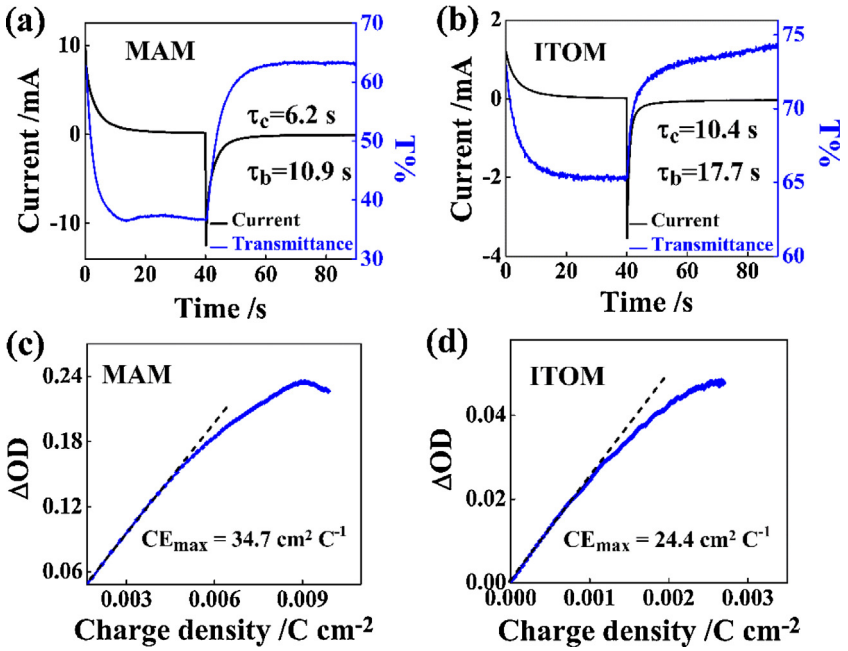

Fig. 3. *In-situ* corresponding transmittance (528 nm) and chronocoulometry switching of (a) MAM and (b) ITOM films on PET under potential steps from –0.45 V (40 s) to 0.5 V (50 s, vs. Ag/AgCl) and optical density at 528 nm of (c) MAM and (d) ITOM, as a function of charge density.

revealed that the room temperature–deposited MAM films are amorphous, as no significant crystalline phase were observed in the obtained XRD patterns (Fig. S4). It has been demonstrated that amorphous MoO_3 film is a more promising material for use in memory devices compared to crystalline MoO_3 because the strongly disordered and loose structure of amorphous MoO_3 film allows facile ion intercalation/deintercalation, allowing for rapid changes of its optical properties [30]. Fig. 4 shows AFM images of MAM and ITOM films, which show that the MAM film on a PET substrate has a noticeably smooth and uniform surface morphology with a root mean square (RMS) roughness of 1.6 nm, similar to that of flexible ITOM films (1.4 nm). There is no sign of aggressive MoO_3 molecules even on the flexible PET substrate, which would have a beneficial effect on the high conductivity and uniform diffusion of electrolytes into the MoO_3 layer [31]. In contrast, the reported flexible WAW films displayed an extremely rough surface with a RMS value of 10.7 nm, which could obviously reduce the continuity of a 10 nm Ag layer and enhance the sheet resistivity of the WAW films. This improvement in surface roughness could be attributed to the use of high–energy ion–beam assistance during the film deposition, which can increase the film compactness and smoothness [22,23].

Coloration efficiency (*CE*) is also an important criterion for assessing EC materials: it is defined as the change in the optical density (*OD*) per unit of inserted charge and can be calculated according to Eq. (1):

$$CE = \Delta OD / \Delta Q = \log(T_b/T_c) / \Delta Q \quad (1)$$

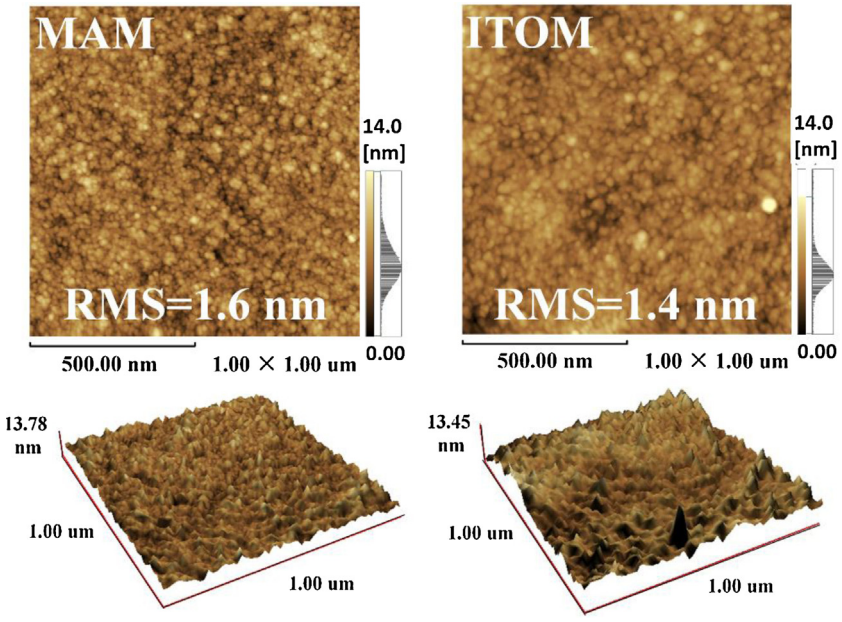

Fig. 4. AFM images of the MAM (30/11/50 nm) and ITOM (50 nm) films deposited on PET substrates.

where ΔQ is the inserted charge that promotes ΔOD in the optical absorbance, and T_b and T_c refer to the bleached and colored transmittance values at a set wavelength, respectively. The calculated CE from the slope of the linear region of the OD-ΔQ curve is 34.7 $cm^2\,C^{-1}$ for the MAM (Fig. 3c), which is nearly 15% larger than that of ITOM (24.4 $cm^2\,C^{-1}$, Fig. 3d) and among the best reported values for MoO_3 [21,32].

To appraise the overall EC performances of the EC films, we calculated a quality factor $\Gamma_{(\lambda)}$ as shown in Eq. (2):

$$\Gamma_{(\lambda)} = CE_{(\lambda)}/\tau,\ \tau = (\tau_c + \tau_b)/2 \quad (2)$$

It stands to reason that a greater Γ denotes better EC performance. The value of $\Gamma_{(528nm)}$ for a MAM film is 4.06 $cm^2\,C^{-1}\,s^{-1}$, which is 2.3 times as high as that of ITOM (1.74 $cm^2\,C^{-1}\,s^{-1}$). This suggests that the EC performance of the flexible MAM film is better than that of the ITOM film.

This improvement in the EC performance for MAM over ITOM could be mainly attributed to its low resistivity (12.5 $\Omega\,\square^{-1}$ for MAM vs. 31.5 $\Omega\,\square^{-1}$ for ITOM). It has been established that electrode resistance has a prominent effect on the EC performance of an ECD, and a high electrode resistance leads to a non-uniform potential across the electrode (ohmic loss), and a non-uniform current distribution in the electrolyte [9,21], which all have a clear impact on the EC properties of the ECD. Moreover, a significant difference in adhesion of the outer MoO_3 layer was observed when the MAM and ITOM films were stuck with scotch tape. Fig. S5 compares the optical microscopy images of these films before and after peeling. As shown, the MAM film retains almost the entire MoO_3 layer, whereas considerable zones of the film were detached in the case of the ITO electrode. The robust construction of the MAM film is more resistant to erosion and improves the cycling durability to a certain extent. In addition, electron transfer from Ag to MoO_3 can be facilitated due to the Fermi level alignment and favorable band bending at the interface between Ag and MoO_3 [24,33].

3.3. Flexibility and EC durability

The fast response time, large optical contrast, and high CE of MAMs suggests a significant improvement in charge utilization, which can desirably induce long-term cycling stability. As shown in Fig. 5a, the MAM film maintains its transmittance modulation ability even after 150 successive step cycles. In contrast, the ITOM becomes almost inactive after only 30 cycles, with the contrast ratio being significantly reduced from 11% to <4%. From the optical microscopy images of the MAM and ITOM films after 150 switching cycles (Fig. S5), some dark regions appeared on the ITOM film, which could be attributed to self-dissolution or degradation of the surface layer after prolonged cycling. This phenomenon could be averted by adding a protecting layer on top of the film, and further investigations into this hypothesis are underway.

Besides the electrochemical durability, the stability of these flexible films under different temperatures, humidity, environmental conditions, and mechanical stress has a significant effect on the performance of flexible devices. The sheet-resistance stability of the MAM film was investigated as a function of temperature and humidity by annealing the MAM film or exposing it to a controlled environment with a constant temperature of 60 °C and relative humidity (RH) of 90% for 24 h (Fig. S6). We observed that after leaving the MAM film exposed to air for 3 months, its sheet resistance only increased by approximately 0.2%. After annealing, the sheet resistance of the MAM increased slightly with increased annealing temperatures up to 250 °C. However, the sheet resistance of the MAM film was dramatically enhanced after annealing at 300 °C for 30 min, which may be the result of Ag oxidization caused by heating. However, the MAM film has good thermal stability over a certain temperature range, and has excellent stability with regards to moisture. The sheet resistance is slightly enhanced by only 1% after being stored at 60 °C, 90% RH for 24 h. For comparison, the resistivity of an 11 nm Ag layer under the same condition increased by 30%, which illustrates that the MoO_3 layer can effectively protect an Ag layer. These results demonstrate that the MAM electrode exhibits good thermal, moisture, and environmental stability, and is suitable for use in stable and efficient ECDs.

The MAM film not only has excellent electrical and optical properties, but it has promising mechanical properties as well. Fig. 5b shows how the resistances of the MAM and ITOM films change following repeated bending at an 11 mm radius of curvature. For MAM films, the resistance only slightly increases

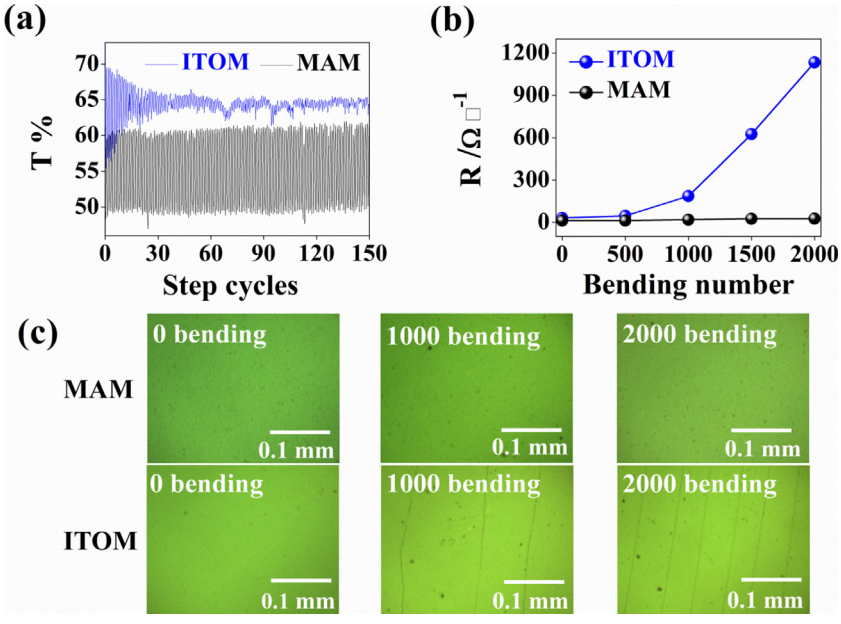

Fig. 5. (a) *In-situ* optical transmittance modulation for flexible MAM and ITOM films on PET at 528 nm at potentials of –0.45–0.5 V; (b) Changes in resistivity values and (c) Optical microscopy images (×200 magnification) of the MAM and ITOM films on PET after repeated bending at an 11 mm radius of curvature.

from 12.5 to 26.7 $\Omega\,\square^{-1}$ after 2000 bending cycles. In contrast, the resistance of ITOM increases dramatically from 31.5 to 1134 $\Omega\,\square^{-1}$ under the same conditions, which is due to the inherent brittleness of ITO. Fig. 5c shows optical microscopy images of the MAM and ITOM surfaces before and after 1000 and 2000 bending cycles. We can see that the MAM surface features remain almost unchanged even after 2000 cycles. By comparison, a few cracks appear at the surface of ITOM after 1000 cycles and become more prominent after 2000 cycles, which could be caused by internal film stress [34].

The EC performances of MAM and ITOM after 1000 and 2000 bending cycles were also studied in order to compare their mechanical stabilities, the details of which are summarized in Table S3 and Fig. S7. We found that the increased resistivity and cracks developed by the ITOM films after bending induced a remarkable decrease in the current density of 60%, transmittance excursion in the bleached state, and a notable decrease (30%) in the optical contrast (Fig. S7). In contrast, the current-time curve and optical transmittance modulation curve for the MAM films are nearly indistinguishable before and after the bending tests, indicating that the MAM films have advanced mechanical stability and great potential application in robust flexible ECDs.

4. Conclusions

In summary, by employing a bi-functional stacked MAM film as both an electrode and EC film, we demonstrated high-performance, flexible ITO-free ECDs. We found that the stacked MAM structure was effective at decreasing the response time, improving the optical modulation, and evaluating the CE of MoO_3 layers compared to a similar ITOM construction. Most importantly, a significant enhancement in the electrochemical and mechanical durability of the MoO_3 film was achieved in the MAM structure. These improvements are based on the high conductivity, good cohesion and homogeneity, suitable energy alignment, and perfect robustness of the MAM film. The mass production of MAM structures on flexible substrates using roll-to-roll magnetron sputtering technologies can be realized. Therefore, this low-cost and room-temperature-deposited dual-function MAM film has great potential for use in efficient and large-area flexible ECDs.

Acknowledgments

This work is supported by the Innovation Program of Chinese Academy of Sciences (CAS), and National Natural Science Foundation of China No. 6140031454, and project supported by State Key Laboratory of Luminescence and Applications.

Appendix A. Supplementary data

Supplementary data associated with this article can be found, in the online version, at http://dx.doi.org/10.1016/j.electacta.2015.12.115.

References

[1] A. Llordes, G. Garcia, J. Gazquez, D.J. Milliron, Tunable near-infrared and visible-light transmittance in nanocrystal-in-glass composites, Nature 500 (2013) 323.
[2] Y.X. Wei, J.L. Zhou, J.M. Zheng, C.Y. Xu, Improved stability of electrochromic devices using Ti-doped V_2O_5 film, Electrochim. Acta 166 (2015) 277–284.
[3] M. Wang, K.J. Koski, Reversible chemochromic MoO_3 nanoribbons through zerovalent Metal Intercalation, ACS Nano 9 (2015) 3226–3233.
[4] L.M.N. Assis, L. Ponez, A. Januszko, K. Grudzinski, A. Pawlicka, A green-yellow reflective electrochromic device, Electrochim. Acta 111 (2013) 299–304.
[5] M.A. Invernale, Y.J. Ding, G.A. Sotzing, All-organic electrochromic spandex, ACS Appl. Mater. Interfaces 2 (2010) 296–300.
[6] Y.M. Zhu, M.T. Otley, X.Z. Zhang, M.F. Li, C. Asemota, G. Li, M.A. Invernalea, G.A. Sotzing, Polyelectrolytes exceeding ITO flexibility in electrochromic devices, J. Mater. Chem. C 2 (2014) 9874–9881.
[7] W. Yu, L. Shen, F. Meng, Y. Long, S. Ruan, W. Chen, Effects of the optical microcavity on the performance of ITO-free polymer solar cells with WO_3/Ag/WO_3 transparent electrode, Sol. Energy Mater. Sol. Cells 100 (2012) 226–230.
[8] E.O. Polat, O. Balci, C. Kocabas, Graphene based flexible electrochromic devices, Sci Rep 4 (2014) 6484.
[9] K. Wang, H.P. Wu, Y.N. Meng, Y.J. Zhang, Z.X. Wei, Integrated energy storage and electrochromic function in one flexible device: an energy storage smart window, Energy Environ. Sci. 5 (2012) 8384–8389.
[10] J. Jensen, M. Hosel, I. Kim, J.S. Yu, J. Jo, F.C. Krebs, Fast switching ITO free electrochromic devices, Adv. Funct. Mater. 24 (2014) 1228–1233.
[11] J. Jensen, M. Hosel, A.L. Dyer, F.C. Krebs, Development and manufacture of polymer-based electrochromic devices, Adv. Funct. Mater. 25 (2015) 2073–2090.
[12] Klaus Ellmer, Past achievements and future challenges in the development of optically transparent electrodes, Nat. Photonics 6 (2012) 808–816.
[13] B.L. Tian, G. Williams, D.Y. Ban, H. Aziz, Transparent organic light-emitting devices using a MoO_3/Ag/MoO_3 cathode, J. Appl. Phys. 110 (2011) 104507.
[14] C. Tao, G. Xie, C. Liu, X. Zhang, W. Dong, F. Meng, X. Kong, L. Shen, S. Ruan, W. Chen, Semitransparent inverted polymer solar cells with MoO_3/Ag/MoO_3 as transparent electrode, Appl. Phys. Lett. 95 (2009) 053303.
[15] L. Cattin, M. Morsli, F. Dahou, S.Y. Abe, A. Khelil, J.C. Bernede, Investigation of low resistance transparent MoO_3/Ag/MoO_3 multilayer and application as anode in organic solar cells, Thin Solid Films 518 (2010) 4560–4563.
[16] H.L. Li, Y. Lv, X. Zhang, X.Y. Wang, X.Y. Liu, High-performance ITO-free electrochromic films based on bi-functional stacked WO_3/Ag/WO_3 structures, Sol. Energy Mater. Sol. Cells 136 (2015) 86–91.
[17] S. Saji, C.W. Lee, Molybdenum, molybdenum oxides, and their electrochemistry, Chemsuschem 5 (2012) 1146–1161.
[18] T. Brezesinski, J. Wang, S.H. Tolbert, B. Dunn, Ordered mesoporous alpha-MoO_3 with iso-oriented nanocrystalline walls for thin-film pseudocapacitors, Nat. Mater. 9 (2010) 146–151.
[19] C.S. Hsu, C.C. Chan, H.T. Huang, C.H. Peng, W.C. Hsu, Electrochromic properties of nanocrystalline MoO_3 thin films, Thin Solid Films 516 (2008) 4839–4844.
[20] B. Dasgupta, Y. Ren, L.M. Wong, L.Y. Kong, E.S. Tok, W.K. Chim, S.Y. Chiam, Detrimental effects of oxygen vacancies in electrochromic molybdenum oxide, J. Phys. Chem. C 119 (2015) 10592–10601.
[21] Z.C. Wang, X.F. Hu, U. Helmersson, Peroxo sol-gel preparation: photochromic/electrochromic properties of Mo-Ti oxide gels and thin films, J. Mater. Chem. 10 (2000) 2396–2400.
[22] C. Yang, H.Q. Fan, Y.X. Xi, J. Chen, Z. Li, Effects of depositing temperatures on structure and optical properties of TiO_2 film deposited by ion beam assisted electron beam evaporation, Appl. Surf. Sci. 254 (2008) 2685–2689.
[23] R. Thielsch, A. Gatto, J. Heber, N. Kaiser, A comparative study of the UV optical and structural properties of SiO_2, Al_2O_3, and HfO_2 single layers deposited by reactive evaporation ion-assisted deposition and plasma ion-assisted deposition, Thin Solid Films 410 (2002) 86–93.
[24] D.T. Nguyen, S. Vedraine, L. Cattin, P. Torchio, M. Morsli, F. Flory, J.C. Bernede, Effect of the thickness of the MoO_3 layers on optical properties of MoO_3/Ag/MoO_3 multilayer structures, J. Appl. Phys 112 (2012) 63505.
[25] N. Zhang, Y. Hu, X. Liu, Transparent organic thin film transistors with WO_3/Ag/WO_3 source-drain electrodes fabricated by thermal evaporation, Appl. Phys. Lett 103 (2013) 033301.
[26] L. Cattin, Y. Lare, M. Makha, M. Fleury, F. Chandezon, T. Abachi, M. Morsli, K. Napo, M. Addou, J.C. Bernède, Effect of the Ag deposition rate on the properties of conductive transparent MoO_3/Ag/MoO_3 multilayers, Sol. Energy Mater. Sol. Cells 117 (2013) 103–109.
[27] L. Cattin, J.C. Bernede, M. Morsli, Toward indium-free optoelectronic devices: Dielectric/metal/dielectric alternative transparent conductive electrode in organic photovoltaic cells, Phys. Status Solidi A-Appl. Mat. 210 (2013) 1047–1061.
[28] M. Hepel, H. Redmond, I. Dela, Electrochromic WO_{3-x} films with reduced lattice deformation stress and fast response time, Electrochim. Acta 52 (2007) 3541–3549.
[29] M. Hepel, H. Redmond, Large cation model of dissociative reduction of electrochromic WO_{3-x} films, Cent. Eur. J. Chem 7 (2009) 234–245.
[30] Y.A. Yang, Y.W. Cao, B.H. Loo, J.N. Yao, Microstructures of electrochromic MoO_3 thin films colored by injection of different cations, J. Phys. Chem. B 102 (1998) 9392–9396.
[31] N.P. Logeeswaran, M.S. Kobayashi, W. Islam, P. Wu, N.X. Chaturvedi, S.Y. Fang, R. S.Williams Wang, Ultrasmooth silver thin films deposited with a germanium nucleation layer, Nano Lett. 9 (2009) 178–182.
[32] D.D. Yao, R.A. Rani, A.P. O'Mullane, K. Kalantar-zadeh, J.Z. Ou, Enhanced coloration efficiency for electrochromic devices based on anodized Nb_2O_5/electrodeposited MoO_3 binary systems, J. Phys. Chem. C 118 (2014) 10867–10873.
[33] S. Balendhran, S. Walia, M. Alsaif, E.P. Nguyen, J.Z. Ou, S. Zhuiykov, S. Sriram, M. Bhaskaran, K. Kalantar-zadeh, Field effect biosensing platform based on 2D alpha-MoO_3, ACS Nano 7 (2013) 9753–9760.
[34] Z. Qi, J. Cao, L. Ding, J. Wang, Transparent and transferrable organic optoelectronic devices based on WO_3/Ag/WO_3 electrodes, Appl. Phys. Lett 106 (2015) 053304.